Dalton Transactions

ROYAL SOCIETY OF CHEMISTRY

PAPER

View Article Online
View Journal | View Issue

Cite this: *Dalton Trans.*, 2025, **54**, 17137

Dual deoxygenation in an α-ketoimine chelated rhenium(III) complex: structural and mechanistic interpretations†

Ankita Sinha,[a] Suparna Banerjee,[b] Suphal Sen,[c] Aniruddha Ghosh,[a] Arindam Dey,[a] Tilak Naskar,[d] Tejender Singh*[e] and Jaydip Gangopadhyay *[a]

An unprecedented case of dual deoxygenation is demonstrated in rhenium chemistry. It is authenticated that an oxorhenium(V) motif and a chelated diaryl-α-ketooxime ligand undergo concurrent oxygen atom transfer (OAT) to form a triarylphosphine oxide coordinated Re^{III}–α-ketoimine complex. The two OAT events are mutually dependent. OAT-induced $Re^{V}{=}O \rightarrow Re^{III}{-}OPR_3$ conversion must occur prior to the OAT-mediated α-ketooxime → α-ketoimine transformation. The first intramolecular OAT occurs across a free energy barrier of 29.1 kcal mol^{-1}, and subjacent molecular orbital effects related to $Ph_3P \rightarrow \pi^*_{Re{=}O}$ charge transfer are identified. The N–O bond cleavage of the oxime is induced by oxidative addition at the Re^{III} centre across a free energy barrier of 25.8 kcal mol^{-1} to afford a reactive Re^{V}–hydroxo intermediate. The second intramolecular OAT involves electron transfer between the Re^{V}-bound hydroxo and PPh_3 moieties. Due to increased nucleophilicity of the hydroxo group, the second OAT is kinetically facile, with a low activation barrier of 8.3 kcal mol^{-1}. Interestingly, while PPh_3 acts as a nucleophile in the first OAT, it behaves as an electrophile in the second. Deoxygenation of diaryl-α-ketooxime is halted upon replacing the oxorhenium(V) motif by a kinetically nonlabile imidorhenium(V) moiety in the Re^{V}–precursor. In that case, deprotonation of oxime occurs exclusively to generate the Re^{V}–α-ketooximato complex. The predominance of the C-nitroso form of the oxime in the Re^{V}–α-ketooximato species is a notable and hitherto unreported feature in rhenium chemistry. The aforementioned reactions of diaryl-α-ketooxime elegantly highlight Re^{V}-substrate selectivity, which is justified through comprehensive mechanistic analysis.

Received 28th July 2025,
Accepted 16th October 2025

DOI: 10.1039/d5dt01782c

rsc.li/dalton

Introduction

Metal-promoted activation and functionalisation of oximes constitute an intriguing domain of chemical research, as metals with variable oxidation states are capable of exerting varying influences on the electrophilicity/nucleophilicity, acidity/basicity and redox behaviours of oximes.[1–4] We verified that structurally authenticated examples of rhenium-promoted functionalisation of oximes are scarce, and only a handful have been reported to date. Structural evidence for N- and O-functionalisation of oximes in rhenium complexes have been provided for (i) the oxidative addition of acetoxime to a Re(I) precursor, yielding Re(III)-iminato species;[5] (ii) the addition of ketoximes across the C≡N bond in *cis*-$[Re^{IV}Cl_4(MeCN)_2]$ to generate iminoacylated products;[6] (iii) the insertion of $C_2(CN)_4$ into the Re–O bond of an O-acetoximato-bound Re(I) complex;[7] (iv) the deoxygenation of salicylaldoxime[8] and azooxime,[9] affording their corresponding Re(V)-imine species; and (v) the reduction of boron-capped tris-dioximate Re(III)-semiclathrochelate into its diimine-iminoximate derivative.[10] In none of the aforementioned reports were mechanistic studies explored, except for some tentative propositions. This essentially creates a lacuna in understanding the stepwise progress of these reactions.

Unlike the chemical versatility of aldoximes, ketoximes and dioximes,[1,2,4] the reactions of α-ketooximes have primarily been studied in the context of the spectrophotometric determination of various transition-metal ions.[11] Documentation of the coordination chemistry of α-ketooximes is mostly limited to the lighter 3d metals to date,[12–17] and only limited attention has been paid to their chemistry with post-lanthanide tran-

[a]*Department of Chemistry, St. Paul's Cathedral Mission College, University of Calcutta, 33/1 Raja Rammohan Roy Sarani, Kolkata 700009, India. E-mail: gjaydip@rediffmail.com*
[b]*Department of Chemistry, Uluberia College, University of Calcutta, Howrah 711315, India*
[c]*School of Advanced Sciences, Vellore Institute of Technology, Tamil Nadu 632014, India*
[d]*Department of Chemistry, IIT Gandhinagar, Gujarat 382355, India*
[e]*Tata Institute of Fundamental Research, Hyderabad 500046, India. E-mail: tej.sts99@gmail.com*

† Dedicated in loving memory of Prof. Amalesh Chandra Banerjee.

sition metals. To the best of our knowledge, α-ketooximes have not yet been explored in relation to the coordination chemistry of rhenium. This prompted us to investigate a few chemical reactions between a selected diaryl-α-ketooxime (benzilmonoxime, $C_{14}H_{10}O_{keto}NOH$, LNOH where L = $C_{14}H_{10}O_{keto}$) and some specific oxo- and imido-Re^{V}–precursors. All the executed reactions and their products are depicted in Scheme 1 as an overview. The observed reactions showcase N- and O-functionalisations of LNOH upon chelation to rhenium. Depending on the nature of the metal precursor employed, LNOH furnishes triarylphosphine oxide coordinated Re^{III}–diaryl-α-ketoimines (**1** and **2**) incorporating LNH chelation, and a Re^{V}–diaryl-α-ketooximato (**3**) product featuring LNO^{-} chelation.

Oxime → imine transformation in the presence of PPh_3 is also discernible for a couple of other reactions in rhenium chemistry: (i) between $[Re^{V}OCl_3(PPh_3)_2]$ and salicylaldoxime,[8] and (ii) between $[Re^{V}(NC_6H_5)Cl_3(PPh_3)_2]$ and phenylazooxime.[9] In these two reactions, the resulting Re^{V}-imine products retain the structural integrity of the $[Re{\equiv}O]^{3+}$ and $[Re{\equiv}NC_6H_5]^{3+}$ moieties. Therefore, oxime-centred deoxygenation *via* single outward oxygen atom transfer (OAT) is common in both reactions.

In contrast, the formation of **1** from $[Re^{V}OCl_3(PPh_3)_2]$ in our case is clearly the manifestation of the harmonious interplay of two outward OAT events, *viz.* $[Re^{V}{\equiv}O]^{3+} \rightarrow [Re^{III}{-}OPPh_3]^{3+}$ and LNOH → LNH, resulting in the loss of the structural identities of the $[Re^{V}{\equiv}O]^{3+}$ and LNOH fragments. Interestingly, $[Re^{V}{\equiv}O]^{3+} \rightarrow [Re^{III}{-}OPPh_3]^{3+}$ two-electron reduction indicates incomplete outward OAT in the primary coordination sphere, while LNOH → LNH two-electron reduction corroborates complete outward OAT in the secondary coordination sphere. Therefore, the first example of metal- and oxime-centred dual deoxygenation in rhenium chemistry is demonstrated upon the successful isolation and characterisation of **1** and **2**. Again, the deprotonation of diaryl-α-ketooxime upon reaction with $[Re^{V}(NC_6H_4Cl)Cl_3(PPh_3)_2]$ in our case is in sharp contrast with the deoxygenation of phenylazooxime reported earlier.[9] Such substrate-selective reactivity of the diaryl-α-ketooxime and oxime-specific product formation from $[Re^{V}OCl_3(PPh_3)_2]$ are explained herein.

To understand the substrate-selective reactivity of the diaryl-α-ketooxime ligand, a comprehensive mechanistic study is carried out computationally. The expounded mechanism can also provide insight into the difference in chemical behaviours of salicylaldoxime and diaryl-α-ketooxime towards the $[ReOCl_3(PPh_3)_2]$ precursor. Structural authentication of **1** and **3** alongside the mechanism can further shed light on the catalytic reactions, such as the dehydration of aldoximes into nitriles,[18] the Beckmann rearrangement of ketoximes into

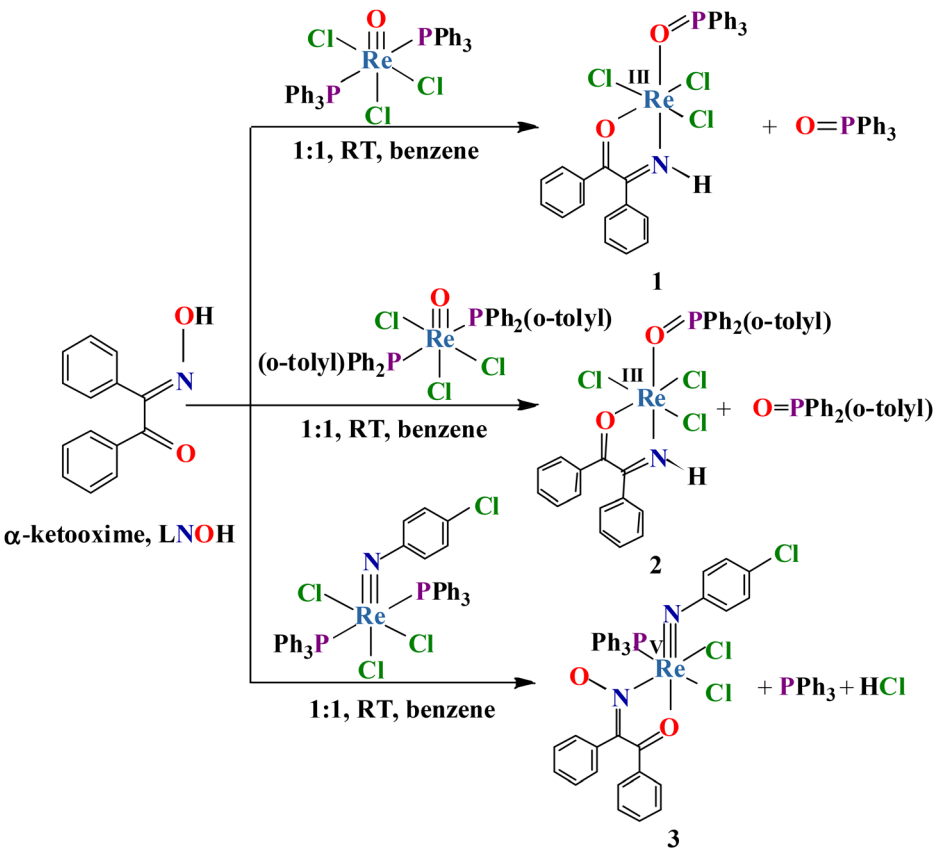

Scheme 1 An overview of the reactions between LNOH and different Re^{V}–precursors, affording **1**, **2** and **3**.

amides,[19,20] the reduction of perchlorate into chloride,[21–25] and the deoxydehydration of alcohols to olefins,[26] promoted by rhenium complexes. Moreover, the complexes may show promise as abiological models to delve deeper into Mo-mediated OAT process,[27,28] which plays a pivotal role in the functioning of biologically important Mo-oxotransferase metalloenzymes.[29]

Experimental

Materials and physical measurements

The reagents, such as triphenylphosphine, diphenyl(*o*-tolyl) phosphine, benzil, *p*-chloroaniline and hydroxylamine hydrochloride, were procured from Avra Synthesis. Potassium perrhenate was purchased from Thermo Fisher Scientific. Following the standard procedures, commercially available solvents were dried and distilled before use. The starting materials $[ReOCl_3(PPh_3)_2]$ and $[Re(NC_6H_4Cl\text{-}p)Cl_3(PPh_3)_2]$ were synthesized following the reported procedures.[30,31] The other oxorhenium(v) precursor, *i.e.* $[ReOCl_3(PPh_2(o\text{-tolyl}))_2]$, was synthesized following a reported procedure[32] with necessary adjustments. α-Benzilmonoxime was prepared following the literature procedure.[33]

The NMR spectra were recorded on a Bruker Avance Neo 400 MHz spectrometer in $CDCl_3$ solvent. The spin–spin structures are abbreviated as follows: s, singlet; d, doublet; t, triplet; and m, multiplet. A PerkinElmer 2400 II elemental analyser was used for microanalysis purposes.

Synthesis of 1

50 mg (0.06 mmol) of $[ReOCl_3(PPh_3)_2]$ was gradually dissolved under stirring in 70 mL of warm benzene to obtain a greenish yellow solution. The solution was then brought to room temperature, into which 14 mg (0.06 mmol) of solid α-benzilmonoxime (LNOH) was added. The mixture immediately became violet and then turned yellowish brown. During a stirring period of 45 min at room temperature, the solution appeared brownish green. The solution thus obtained was then directly subjected to column chromatography on a silica gel bed (20 × 1 cm, 60–120 mesh). A green band was eluted with dichloromethane. Solvent removal from the eluate under slow evaporation afforded the green-coloured $[Re(OPPh_3)Cl_3(LNH)]$ complex (**1**), which was washed twice (5 mL each) with diethyl ether. Compound **1** is thermally unstable and cannot be recovered from the eluate under reduced pressure using a rotary evaporator. It also gradually decomposes in the solid state over three days when exposed to air. Single crystals were obtained from the slow diffusion of a dichloromethane solution of **1** into hexane inside a refrigerator. Yield: 30 mg (64%).

Synthesis of 2

The brownish-yellow complex **2** was synthesised following the same procedure as described for **1**, except that the $[ReOCl_3(PPh_2(o\text{-tolyl}))_2]$ precursor was used instead of $[ReOCl_3(PPh_3)_2]$. Yield: 28 mg (62%).

Synthesis of 3

66 mg (0.07 mmol) of $[Re(NC_6H_4Cl)Cl_3(PPh_3)_2]$ was gradually dissolved in 75 mL of warm benzene under stirring to get a bottle-green solution. The solution was allowed to cool to ambient temperature. 16 mg (0.07 mmol) of solid α-benzilmonoxime (LNOH) was then added to the metal precursor solution. The mixture was then stirred for 2 h. Over this time, the solution gradually turned brown-green in colour. The solvent was then removed under reduced pressure and washed thrice (5 mL each) with hexane. The dark mass thus obtained was then subjected to column chromatography on a silica gel bed (25 × 1 cm, 60–120 mesh). A brown-green band was eluted with a benzene-acetonitrile (10 : 1) mixture. Solvent removal from the eluate under reduced pressure afforded the brownish-green-coloured $[Re(NC_6H_4Cl)Cl_3(LNO^-)]$ complex (**3**). Unlike **1**, this complex is indefinitely stable in air. Single crystals were obtained from the slow diffusion of a dichloromethane solution of **3** into hexane. Yield: 51 mg (76%).

Analytical data for 1. Anal. calcd (%) for $C_{32}H_{26}Cl_3NO_2PRe$: C, 49.23; H, 3.33; N, 1.79. Found: C, 49.01; H, 3.06; N, 1.56. ^{1}H NMR (400 MHz, δ, ppm): 8.43 (s, 1H), 8.10 (d, J = 8.0 Hz, 1H), 8.04 (d, J = 8.0 Hz, 2H) 8.00 (d, J = 8.0 Hz, 2H), 7.43–7.71 (m, 14H), 7.15 (t, J = 8.0 Hz, 2H), 6.96 (d, J = 8.0 Hz, 2H), 6.81–6.84 (m, 2H).

Analytical data for 2. Anal. calcd (%) for $C_{33}H_{28}Cl_3NO_2PRe$: C, 49.47; H, 3.36; N, 1.75. Found: C, 49.32; H, 3.09; N, 1.61. ^{1}H NMR (400 MHz, δ, ppm): 9.71 (d, J = 8.0 Hz, 1H), 9.60 (t, J = 6.0 Hz, 1H), 9.55 (t, J = 8.0 Hz, 1H), 9.14 (t, J = 8.0 Hz, 2H), 8.92 (s, 1H), 8.01 (t, J = 8.0 Hz, 2H), 6.83–7.96 (m, 11H), 5.48 (t, J = 6.0 Hz, 1H), 4.59 (t, J = 8.0 Hz, 2H), 2.80 (s, 3H), −2.22 (t, J = 8.0 Hz, 1H).

Analytical data for 3. Anal. calcd (%) for $C_{38}H_{29}Cl_3N_2O_2PRe$: C, 47.79; H, 3.04; N, 2.93. Found: C, 47.48; H, 2.95; N, 2.79. ^{1}H NMR (400 MHz, δ, ppm): 7.29–7.65 (m, 25H), 7.97 (d, J = 8.0 Hz, 2H), 8.05 (d, J = 8.0 Hz, 2H).

Crystallography

Intensity data from single crystals of **1** and **3** were collected on a Bruker APEX-II CCD X-ray diffractometer equipped with Mo-Kα radiation (λ = 0.71073 Å). The corresponding structures of **1** and **3** were generated by the SHELXT program[34] and subsequently refined by the full matrix least-squares method based on F^2 with the SHELXL package.[35,36] Except for the imine hydrogen atom, which was located from the difference Fourier map and treated by least-squares refinement, all other hydrogen atoms of **1** were added at their calculated sites and refined with isotropic thermal parameters in a riding model. All the H atoms were placed at their calculated positions for **3** and refined isotropically in a riding model. Anisotropic displacement parameters were assigned to all the non-hydrogen atoms of **1** and **3**. One molecule of CH_2Cl_2, identified from the difference Fourier map, in the asymmetric unit of **3** was found to exhibit positional disorder due to high thermal motion. It was initially modelled through splitting into PARTs followed by employing SADI and EADP restraints. Even after such treat-

ment, the highest residual peak of 1.98 e Å^{-3} was found near a chlorine atom of CH_2Cl_2, and the anisotropic displacement parameters of all the atoms of the disordered solvent were quite high. To circumvent the existing issues with the solvent, masking was finally implemented to remove untoward contributions from residual electron density to the scattering. A mask was calculated, and 151 electrons were found in a volume of 617 Å^3 with two voids per unit cell. The number of electrons corresponds to the presence of one CH_2Cl_2 solvent molecule per asymmetric unit (84 electrons per unit cell), along with some additional residual electron density. Furthermore, a few carbon atoms of the two phenyl rings of the oxime ligand in **3** show large anisotropic displacement parameters. The rotational disorder associated with the two phenyl rings was treated by splitting into PARTs, which leaves the C9–C14 phenyl ring with a 56.6 : 43.4% occupancy ratio and the C2–C7 phenyl ring with a 57.6 : 42.4% occupancy ratio. The SHELXL-compatible constraint AFIX and restraint SIMU were also applied to get desirable planarity for the two phenyl rings. In the ORTEP diagram of **3**, the two concerned phenyl rings are shown only with their higher occupancies.

Molecular graphics were generated using Olex2-1.5 software.[37] Selected crystal data and refinement details for **1** and **3** are summarised in Table 1.

Computational methods

Density functional theory (DFT) calculations were carried out using the Gaussian 16 suite of programs.[38] The M06-L functional[39] was used throughout the work along with the 6-31G(d,p) basis set for non-metals[40] and the SDD basis along with ECP for the rhenium centres.[41] M06-L is a constrained local functional placed at rung 3 of Jacob's Ladder, which shows excellent performance for accurate computations of structures and energies of transition-metal compounds that exhibit sharp and distinct variations in electron densities.[42] This also works reasonably well for assessing the vibrational frequencies of the transition states.[42] In contrast to the best algorithms for nonlocal functionals, the M06-L functional requires a relatively low computational cost without compromising much, with desirable accuracy.[43] Therefore, the M06-L functional is widely preferred for transition-metal-based computations over hybrid DFT methods when using good-quality basis sets.[44] Hence, we restricted our study to M06-L and did not pursue any other functionals. The gas-phase computation seems reasonably acceptable, as the nonpolar benzene used in our synthesis precludes any significant chemical role for solvation. The intermediates and transition states shown in Fig. 3 were identified from optimisation and frequency calculations with zero and one imaginary frequency, respectively. The related Cartesian coordinates of all species are provided in the ESI. QTAIM calculations, an analysis of AO contributions, and Mayer bond order (MBO) analysis were done at the M06-L/6-31G(d,p) level of theory using Multiwfn 3.8 software.[45] NBO analysis and the atomic contributions to the molecular orbitals were calculated at the M06-L/6-31G(d,p) level of theory using the NBO 7.0 program[46] as implemented in the Gaussian package.

Table 1 Selected crystallographic data and refinement parameters for **1** and **3**

Compound	**1**	**3**
Formula	$C_{32}H_{26}Cl_3NO_2PRe$	$C_{39}H_{31}Cl_5N_2O_2PRe$
M (g mol^{-1})	780.06	954.08
Temperature (K)	154.99	297
Crystal system	Monoclinic	Triclinic
Space group	$P2_1/n$	$P\bar{1}$
Crystal size (mm)	0.2 × 0.1 × 0.1	0.2 × 0.1 × 0.1
a (Å)	10.5959(6)	11.0316(9)
b (Å)	19.8922(10)	13.7471(12)
c (Å)	14.4642(7)	15.4809(13)
α, β, λ (°)	90, 90.389(2), 90	75.994(2), 76.868(2), 80.556(2)
V (Å^3), Z	3048.6(3), 4	2203.5(3), 2
ρ_{calc} (g cm^{-3})	1.700	1.438
μ (mm^{-1})	4.331	3.129
Θ range for data collection (°)	2.38 to 25.69	2.30 to 26.34
Index ranges	$-12 \le h \le 12$, $-23 \le k \le 21$, $-17 \le l \le 17$	$-13 \le h \le 13$, $-16 \le k \le 16$, $-18 \le l \le 18$
Total, uniq. data, R_{int}	27439, 5503, 0.0752	49051, 7989, 0.0364
R_1, ωR_2, GoF	0.0430, 0.1054, 1.058	0.0371, 0.0831, 1.160
Largest diff. peak/hole (e Å^{-3})	2.091/−2.261	1.136/−1.497
Radiation (Å)	Mo-Kα, 0.71073	Mo-Kα, 0.71073

Results and discussion

Synthesis and ^{1}H NMR spectra

Under ambient conditions, in benzene, $[Re^{V}OCl_3(PPh_3)_2]$ reacts with LNOH at an equimolar ratio to afford a green Re^{III}–α-ketoimine product, **1**. The $[Re^{V}OCl_3(PPh_2(o\text{-tolyl}))_2]$ precursor, an *in situ* source of a reasonably bulkier PPh_2(*o*-tolyl) oxophile, also yielded a similar brownish yellow Re^{III}–α-ketoimine product, **2**. This suggests that the two outward OAT events can withstand the steric impact caused by an increase in phosphine bulk. The ^{1}H NMR spectra of the two complexes both display well-resolved peaks and complex aromatic multiplets. The downfield ^{1}H NMR singlets at 8.43 and 9.03 ppm mark the presence of deshielded imine protons in **1** and **2**, respectively. The methyl group of the PPh_2(*o*-tolyl) ligand in **2** resonates as a singlet at 2.80 ppm. $[Re^{V}(NC_6H_4Cl)Cl_3(PPh_3)_2]$ reacts with LNOH in benzene to furnish a brownish green Re^{V}–α-ketooximato product, **3**. Substantial overlapping of the individual proton signals in the ^{1}H NMR spectrum of **3** is expressed as ill-resolved aromatic multiplets in the region of 7.3–7.7 ppm.

Crystal structures

Single-crystal X-ray structures of **1** and **3** are ascertained. Selected parameters of **1** and **3** are collected in Tables 2 and 3, respectively. Respective molecular views of **1** and **3** are depicted in Fig. 1 and 2, respectively.

Table 2 Selected parameters for **1**

Bond length (Å)			
Re1–Cl1	2.3459(15)	Re1–O2	2.059(4)
Re1–Cl2	2.3244(16)	O1–C1	1.315(7)
Re1–Cl3	2.3695(15)	N1–C8	1.357(7)
Re1–N1	1.962(4)	N1–H1	0.98(9)
Re1–O1	1.992(4)	C1–C8	1.387(9)
Bond angle (°)			
O1–Re1–Cl3	91.26(12)	P1–O2–Re1	146.0(3)
O1–Re1–O2	94.10(16)	Cl1–Re1–Cl3	175.18(5)
O2–Re1–Cl1	88.53(11)	Cl1–Re1–Cl2	90.23(6)
O2–Re1–Cl2	92.26(12)	Cl2–Re1–Cl3	90.47(6)
O2–Re1–Cl3	86.68(11)	O1–Re1–Cl1	88.57(12)
N1–Re1–Cl1	93.57(15)	O1–Re1–Cl2	173.50(11)
N1–Re1–Cl2	97.55(16)	N1–Re1–O1	76.15(19)
N1–Re1–Cl3	91.06(15)	N1–Re1–O2	169.95(18)

Table 3 Selected parameters for **3**

Bond length (Å)			
Re1–P1	2.4477(13)	Re1–O1	2.040(3)
Re1–Cl1	2.3773(15)	O1–C1	1.305(6)
Re1–Cl2	2.3916(13)	N1–C8	1.395(7)
Re1–N1	2.046(5)	N1–O2	1.251(6)
Re1–N2	1.720(4)	C1–C8	1.386(8)
Bond angle (°)			
Cl1–Re1–P1	86.76(5)	N2–Re1–Cl1	106.09(14)
Cl1–Re1–Cl2	86.76(5)	N2–Re1–Cl2	100.46(14)
Cl2–Re1–P1	169.98(5)	N2–Re1–O1	163.36(16)
O1–Re1–P1	86.20(10)	N2–Re1–N1	90.25(18)
O1–Re1–Cl1	89.43(10)	N1–Re1–P1	97.90(13)
O1–Re1–Cl2	86.10(10)	N1–Re1–Cl1	163.16(13)
O1–Re1–N1	74.82(16)	N1–Re1–Cl2	86.25(13)
N2–Re1–P1	88.69(14)	O2–N1–Re1	123.70(3)

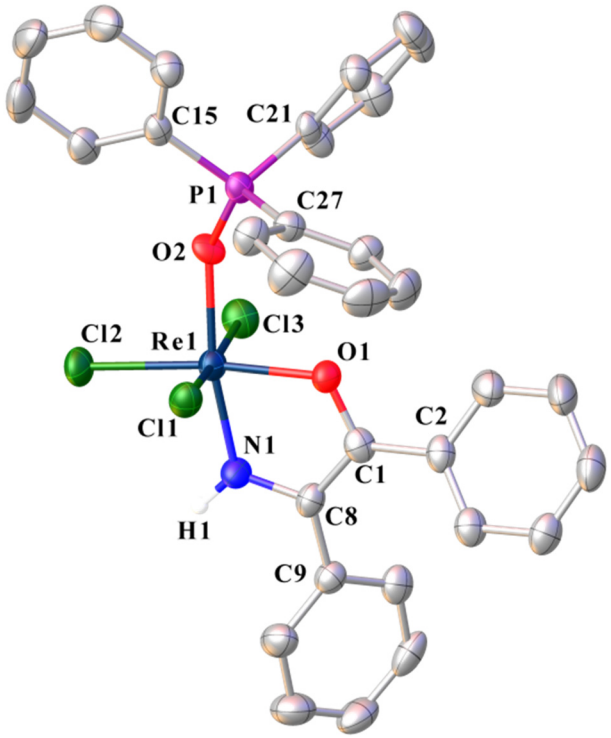

Fig. 1 The ORTEP view (50% probability) of the asymmetric unit of **1**, showing the atom numbering pattern. Except for the imine hydrogen atom (H1), all other H atoms are omitted for clarity.

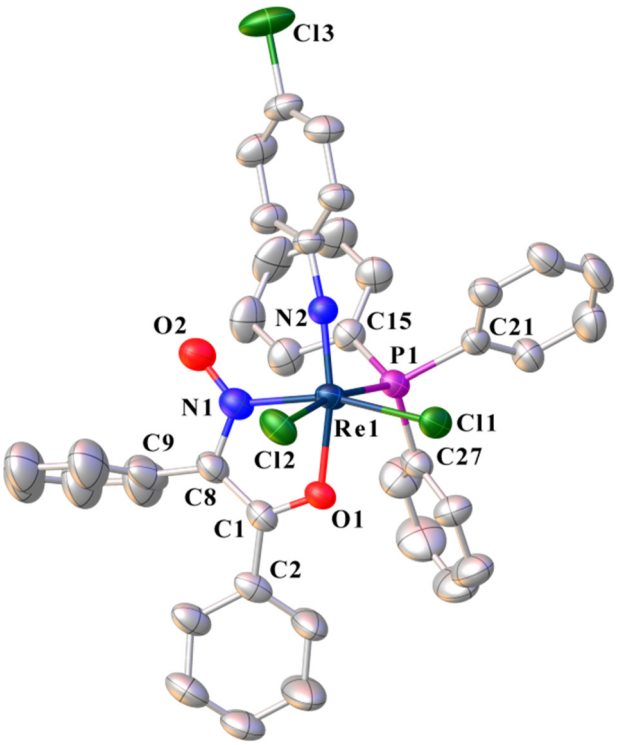

Fig. 2 The ORTEP view (50% probability) of **3** showing the atom numbering pattern. All H atoms are omitted for clarity.

The asymmetric unit of **1** contains an isolated [$Re^{III}(OPPh_3)Cl_3(C_{14}H_{11}NO)$] molecule. Three *meridionally* disposed Cl atoms, an O_{keto} atom and the Re1 atom altogether constitute a distorted equatorial fragment with a root mean square deviation (rmsd) of 0.097 Å from planarity. Axial distortion is also evident, as ∠N1–Re1–O2 is ~10° away from being perfectly linear. The overall deviation from ideal octahedral geometry stems from the significant compression of the LNH bite angle (76.15(19)°). Unlike the equatorial plane, the Re1O1C1C8N1 chelate ring has excellent planarity (rmsd = 0.016 Å), and the two dangling phenyl rings at the C1 and C8 atoms make dihedral angles with it of 27.0° and 45.8°, respectively. The bond attributes of the bent Re–O=PPh_3 motif (Re1–O2 = 2.059(4) Å, ∠P1–O2–Re1 = 146.0(3)°) fall within the normal regime as encountered for other structurally characterised Re^{III}–$OPPh_3$ complexes.[47–50]

Although both the O1 and O2 atoms are sp^2 hybridised from a classical viewpoint, the Re1–O1 bond is nearly 0.07 Å shorter than the Re1–O2 bond. This indicates a stronger binding of the O_{keto} atom of LNH to Re^{III} over $OPPh_3$. The observed difference in binding ability can be ascribed to the moderate π-acceptor behaviour of LNH in contrast to the pure σ-donor nature of $OPPh_3$. Indeed, d_π-electron drift from Re^{III} into the conjugated π^*-orbitals of the Re1O1C1C8N1 chelate ring is confirmed based on the substantial lengthening of the

individual C8═N1 and C1═O1 bonds by *ca.* 0.08 and 0.1 Å, respectively, with concomitant shortening of the C1–C8 bond by ∼0.13 Å compared to their corresponding values in free LNOH.[51] Such measurable $d_{\pi}(Re^{III}) \rightarrow \pi^{*}_{C=O}$ electron delocalisation, in effect, can enhance the π-donor ability of the Cl2 atom lying trans to the O1 atom. Indeed, the Re1–Cl2 bond is shorter than the remaining Re1–Cl1 and Re1–Cl3 bonds by *ca.* 0.02 and 0.04 Å, respectively.

The asymmetric unit of **3** contains a $[Re^{V}(C_6H_4Cl)(PPh_3)Cl_3(C_{14}H_{10}NO_2)]$ molecule and a disordered dichloromethane solvent molecule. Two *cis* Cl atoms, the N1 atom, the P1 atom, and the Re1 atom altogether form an approximately equatorial plane (rmsd = 0.11 Å), from which the Re^{V} atom is shifted towards the N2 atom by 0.19 Å. The roof-like arrangement of the metal and four equatorial atoms stems from strong covalent bonding between the Re^{V} and imido-N2 atoms. The Re1–N2 distance in **3**, 1.720(4) Å, is only slightly longer than an idealised triple-bonded imidorhenium(v) motif.[52,53] The *trans*-influence of the imido group is conspicuously displayed *via* the lengthening of the Re1–O1 bond by ∼0.05 Å over the same bond in **1**. The Re1O1C1C8N1 chelate ring is essentially planar (rmsd = 0.031 Å), and the two pendent phenyl rings at the C1 and C8 atoms form dihedral angles of 15.1° and 78.0°, respectively, with the chelate plane. The bite angle of LNO^{-} is even lower in **3** (74.82(16)°) than observed in **1**, plausibly to suppress undesirable steric congestion with PPh_3. Interestingly, the dihedral angle between the two phenyl rings of LNO^{-} opens up to 74.7° in **3** compared to 62.0° in **1**. Consequently, the O2 atom becomes partially sterically shielded, partly restricting its accessibility by other reagents.

A noteworthy structural feature of the Re^{V}-bound deprotonated oxime in **3** is that the N–O bond is much shorter, by ∼0.15 Å, compared to the length observed in free LNOH.[51] Therefore, an appreciable double-bond character is evident from the short N1–O2 bond length of 1.251(6) Å. This is only possible when the negative charge of the –C═N–O^{-} moiety in LNO^{-} is affected by conjugation and a contribution from the resulting C-nitroso form is dominant. The observed N1–O2 bond length in **3** lies very close to the N–O length of uncoordinated nitrosobenzene (1.240(7) Å)[54] and also excellently matches with nitroso descriptions reported for nitrosoalkane complexes of Fe–porphyrins,[55] nitrosoarene complexes of Fe- and Os-porphyrins,[56,57] and Ru-complexes of 2-(2-nitrosoaryl) pyridine ligands.[58] With augmented covalency in the nitroso group (–N═O), the nitroso-N1 atom is expected to become a relatively weak N-binder to Re^{V} in **3** compared with the bonding of the imine-N1 atom to Re^{III} in **1**. This impression is rightly authenticated by the fact that the Re1–N1 bond in **3** is *ca.* 0.08 Å longer than the same bond in **1**. Furthermore, the electronic effect of the existing C-nitroso form of LNO^{-} is passed on to the C8═N1 bond, and this bond is elongated by *ca.* 0.04 Å in **3** compared to that in **1**.

Mechanistic pathway

Now, elucidation of the reaction mechanism for the dual OAT is essential to understand the sequential steps associated with the formation of triarylphosphine oxide coordinated Re^{III}–α-ketoimine products. The free energy pathway relevant to the $[Re^{V}OCl_3(PPh_3)_2]$ (**A**) → **1** transformation is portrayed in Fig. 3.

LNOH initially undergoes deprotonation under the influence of the metal substrate, and the resulting LNO^{-} can potentially act as an O-nucleophile due to the α-effect.[59] Substitution of a chloride ion in **A** by LNO^{-} is then favoured to yield a η^1-$O_{oximato}$-coordinated Re^{V}-intermediate (**B**) and HCl. Subsequently, **B** transforms into a distorted pentagonal bipyramidal $Re^{V}O$ species (**C**) incorporating the η^2-N,O_{keto} chelation of LNO^{-}. In the optimised structure of **C**, the axial positions are occupied by two chlorine atoms and the approximately pentagonal plane is defined by the oxo moiety,[60] bidentate LNO^{-} and two PPh_3 groups. As observed in other structurally characterised pentagonal bipyramidal $Re^{V}O$ complexes,[61–63] two axial atoms are also bent here (∠Cl(axial)–Re–Cl(axial) = 157.4°) with respect to the basal plane and manifest an average ∠Cl(axial)–Re–O(oxo) value of ∼101.2° with the basal $Re^{V}O$ motif. The computed $Re^{V}O$ distance in **C** is 1.722 Å, suggesting the presence of a triple bond[64] between the two atoms. Weakening of PPh_3 coordination to Re^{V} in **C** is evident from an increase in the average lengths of the two Re^{V}–PPh_3 bonds by ∼0.1 Å compared to **A**.

Natural bond orbital (NBO) analysis[65] affirms that the electronic occupation of the $Re^{V}O$ motif is $\sigma^{1.95}\pi^{1.96}\pi^{1.94}$ in **C**, indicating a triple-bond nature, consistent with the computed bond length value. Two primarily metal-based (70–75%), non-degenerate (−25.9 and −69.2 kcal mol^{-1}), low-lying π^{*}-orbitals of the $Re^{V}O$ motif are therefore available to act as acceptor orbitals in **C**. An occurrence of $Ph_3P \rightarrow \pi^{*}_{ReO}$ charge transfer[47] in **TS1** is computationally validated based on significant π-electron reduction in the ReO motif ($\sigma^{1.91}\pi^{0.96}$). As a consequence of this charge transfer, the Re^{V}≡O bond is found to gradually elongate along the **C** (1.722 Å) → **TS1** (1.951 Å) → **D** (2.176 Å) reaction path, resulting in the first outward OAT. A double bond between the O and P atoms is thus forged to form $OPPh_3$, which remains coordinated to Re^{III}, generating the Re^{III}–$OPPh_3$ intermediate **D**. The free energy barrier for this first OAT is 29.1 kcal mol^{-1}.

A quantum theory of atoms in molecules (QTAIM) study[66] elegantly shows the fluctuations of electron density along the Re···O···P bond path during the course of the $[Re^{V}{\equiv}O]^{3+}$ → $[Re^{III}–OPPh_3]^{3+}$ reaction. The electron density at the bond critical point (BCP, ρ_{BCP}) along the Re–O bond path is 0.2509 a.u. in **C**, which drops to 0.1446 a.u. in **TS1** and further declines to 0.0701 a.u. in **D**. Conversely, electron density reinforcement is attested along the O···P bond path (ρ_{BCP} = 0.1075 a.u. for **TS1** and 0.1952 a.u. for **D**). The advance of OAT is also reflected in a gradual increase in ∠Re–O–PPh_3 from 79.1° in **TS1** to 132.0° in **D**. Two structural attributes of the **D** intermediate, *viz.* ∠Re–O–PPh_3 = 132.0° and $d_{Re–OPPh3}$ = 2.176 Å, mildly deviate from the standard metrical parameters of structurally characterised Re^{III}–$OPPh_3$ complexes.[47–50] Marginally exergonic *trans* → *cis* isomerisation (−0.8 kcal mol^{-1}) of the $ReCl_2$ motif in **D** satisfactorily adjusts the structural parameters of **E** (∠Re–O–PPh_3 =

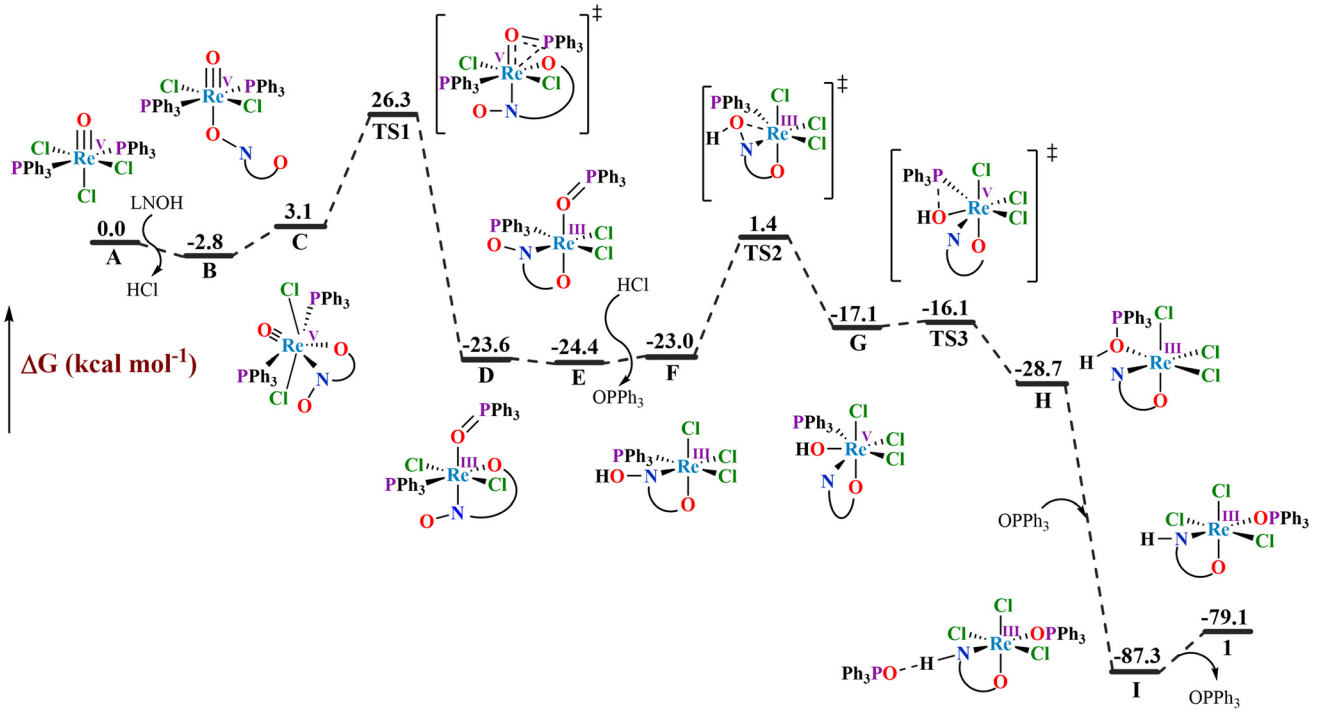

Fig. 3 The free energy diagram for the A → **1** transformation in the gas phase at 298 K. Geometry optimisations were carried out using the M06-L functional and 6-31G(d,p) basis set for the main group elements, while rhenium centres were treated with the SDD basis set and SDD pseudopotential. Single-point energy calculations were carried out with the larger 6-311G(d,p) basis set. Relative free energies are given in kcal mol^{-1}.

145.7°, $d_{Re–OPPh3}$ = 2.103 Å). The X-ray structure of **3** provides compelling evidence related to the existence of **E** in the mechanistic profile due to their structural resemblance, except that the imidorhenium(v) motif in **3** is replaced by a Re^{III}–$OPPh_3$ group in **E**. The exchange of $OPPh_3$ in **E** with HCl forms a new Re^{III}–PPh_3 intermediate, **F**.

The optimised N–OH length (1.372 Å) in **F** aligns well with the structurally characterised N–OH length (1.404 Å) of uncoordinated LNOH.[51] Being deprived of significant double-bond character, the N–OH bond in **F** is susceptible to oxidative addition with the electron-rich Re^{III} centre.[5] NBO analysis exhibits an interesting lone-pair selectivity of the O_{oxime} atom for oxidative addition. The p-rich (>90%) lone pair selectively interacts with the metal, and its occupation depletes to 1.706e in **TS2**. However, the other s-rich (53%) lone pair is reserved in **TS2**, with an occupation of 1.966e.

Oxidative addition occurs *via* weak $Re^{III}\cdots O_{oxime}$ interaction operating at 2.975 Å in **F** (Mayer bond order (MBO): 0.08), which gradually strengthens at a distance of 2.209 Å in **TS2** (MBO: 0.38). Complementarily, as the $Re^{III}\cdots O_{oxime}$ interaction grows, the N–OH bond elongates substantially from 1.372 Å in **F** (MBO = 0.98, ρ_{BCP} = 0.3384 a.u.) to 1.569 Å in **TS2** (MBO = 0.70, ρ_{BCP} = 0.2043 a.u.). The weak-cum-activated N–OH bond in **TS2** finally cleaves to generate the heptacoordinated Re^{V}–OH intermediate **G**. Intermediate **E** reaches **TS2** *via* **F**, surpassing a free energy barrier of 25.8 kcal mol^{-1}.

In the optimised structure of **G**, the Re^{V}–OH bond lying in the pentagonal plane is 2.025 Å long, conforms well with other structurally characterised Re^{V}–O bonds (1.98–2.02 Å) in pentagonal bipyramidal complexes incorporating CH_3O^-,[61] phenolic-O^-, and carboxylic-O^- donors.[62] The Re^{V}–OH bond is composed of 22.6% Re-character and 77.4% O-character and shows $\sigma^{1.92}$ electron occupation. Despite, the HO⋯PPh_3 nonbonded distance (2.653 Å) in the skewed pentagonal plane of **G** is nearly 0.7 Å less than the sum of the van der Waals radii of the O and P atoms;[67] no O⋯P path of interaction exists between them in QTAIM analysis. However, the proximity between the Re^{V}-bound HO and PPh_3 groups in **G** (∠O(basal)–Re–P(basal) = 68.3°) can favour the HO → PPh_3 internal charge transfer. Charge transfer in **TS3** is confirmed by two facts: (i) the shortening of the HO⋯PPh_3 length to 1.702 Å compared to 2.653 Å in **G**, and (ii) the elongation of the Re^{V}–OH bond to 2.263 Å (MBO: 0.29, ρ_{BCP} = 0.0589 a.u.) compared to 2.025 Å (MBO: 0.80, ρ_{BCP} = 0.1187 a.u.) in **G**.

NBO analysis of **TS3** highlights that one lone pair of the OH group present in an $sp^{0.9}$ hybrid orbital donates electrons to the $s^{0.1}p$ antibonding orbital of the P atom in PPh_3. Consequently, the occupancy of the OH-based lone pair depletes markedly to 1.627e, and the P-based antibonding orbital shows a considerable population of 0.638e. The substantial electronic population in the P-based antibonding orbital eventually increases the Re–P bond length from 2.619 Å (**G**) to 3.067 Å (**TS3**). Finally, splitting of the weak Re–P bond forms the Re^{III}–iminato intermediate **H**. The intermediate **E** reaches **TS3** to accomplish the second intramolecular OAT against a free energy barrier of 8.3 kcal mol^{-1}.

Highly exergonic (−58.6 kcal mol^{-1}) **H** → **I** conversion is the final step of the dual deoxygenation process. Three structural issues in **H** deserve scrutiny to probe the huge thermodynamic implications of this transformation. First, the *fac*-$ReCl_3$ disposition in **H** is electronically destabilising, as the *mer*-$ReCl_3$ disposition is ubiquitous in the reported X-ray structures of Cl_3Re^{III}–$OPPh_3$ complexes.[47–50] Second, the stretched Re^{III}–[O(H)PPh_3]$^+$ bond (2.419 Å) is too fragile. Third, the bite angle of LN^- in **H** is drastically low (59.79°), which imposes severe strain on the chelate ring. Therefore, structural reorganisation is much needed. This is achieved by expelling the weakly coordinated [H–O═PPh_3]$^+$ group and allowing rebinding of $OPPh_3$ released in the **E** → **F** step. This forms a *mer*-[$Re^{III}Cl_3$($OPPh_3$)(LN)]$^-$ iminato species and synchronous proton transfer from [H–O═PPh_3]$^+$ yields **I**, which is the H-bonded species of **1** and $OPPh_3$. The formation of **1** is endergonic by 8.2 kcal mol^{-1} with respect to **I** due to the rupture of the appreciably linear and short N–H···O hydrogen bond ($d_{N-H\cdots O}$ = 1.724 Å, ∠N–H···O = 173.63°).

At this stage of discussion, it is conceivable that the $Re^{V}O$ motif in **A** undergoes a plethora of electronic changes (either electron density reinforcement or partial annihilation) in different intermediates and activated states. Therefore, if any trend between the Re–O bond lengths (d_{Re-O}) and ρ_{BCP} values (Table 4) exists,[68] it can serve as an empirical relation to gauge the OAT process of other oxorhenium(v)-promoted functionalisations. Additionally, it can provide insights into the molecular structure and reactivity of any species appearing along the reaction path by analysing its electronic properties at the atomic level, without invoking any orbital interaction approaches. Indeed, an excellent quadratic polynomial fit with a very high coefficient of determination (0.996) is achieved and depicted in Fig. 4. The Re–O_{keto} bonds are not considered in this fit, as they remain almost unaffected by electron redistribution.

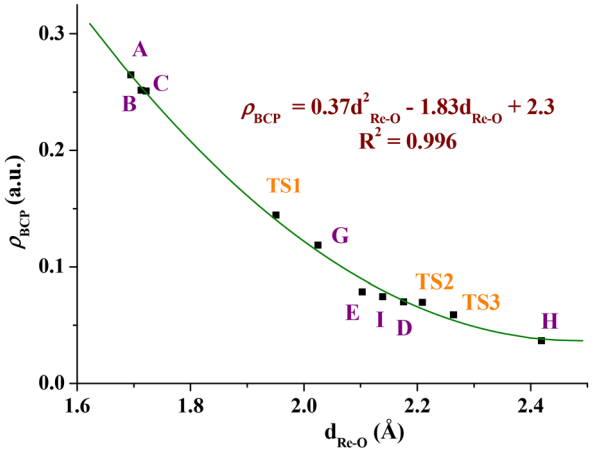

Fig. 4 The second-order polynomial relationship between the ρ_{BCP} (a.u.) and d_{Re-O} (Å) parameters for all species appearing in Fig. 3 except **F** and **1**.

MO perspective of the OAT-induced rate-determining step

The **C** → **D** transformation represents the slowest step of the dual deoxygenation reaction owing to its maximum energy barrier. Therefore, it seems rational to analyse the orbital compositions and energy properties of some MOs of **C** that can influence intramolecular electron transfer during the first OAT. Frontier and secondary molecular orbitals of **C** engaged in electron transfer are depicted in Fig. 5.

Scrutiny of the molecular orbitals of **C** shows that some important occupied orbitals, *viz.* HOMO−3, HOMO−2, HOMO−1 and HOMO are spaced within a sufficiently small energy gap of ∼1 eV. Except for the HOMO (which primarily shows the $5d_{xy}$ character of rhenium), the three other subjacent[69] occupied MOs exhibit σ-type lone-pair electron density localised on the PPh_3 moieties. This σ-type electron density from phosphine must be transferred into the $\pi^*_{Re\equiv O}$ orbital for OAT-driven [Ph_3P–Re^{V}≡O]$^{3+}$ → [Re^{III}–$OPPh_3$]$^{3+}$ conversion to be accomplished. Among the reactive centres in **C**, two P atoms (P1 and P2) show a greater population in the HOMO–1, HOMO–2 and HOMO–3 subjacent orbitals (Table 5). Such a distribution of electron density is expected to facilitate the OAT process by transferring electron density to the $\pi^*_{Re\equiv O}$ virtual orbitals. In search of the acceptor orbitals, we find that all three MOs, *viz.* LUMO, LUMO+1 and LUMO+2 are symmetrically disposed to participate in the electron-transfer process. However, taking account of their relative energies, LUMO and LUMO+1 appear to be suitable to act as potential acceptors.

Based on the symmetry and energy gap between the donor and acceptor MOs, the viable electron transfer pathways in **C** are: (i) HOMO−1 → LUMO (1.79 eV), (ii) HOMO−2 → LUMO (1.93 eV), (iii) HOMO−3 → LUMO (2.21 eV), (iv) HOMO−1 → LUMO+1 (1.97 eV), (v) HOMO−2 → LUMO+1 (2.11 eV) and (vi) HOMO−3 → LUMO+1 (2.39 eV). However, pathways (i), (ii) and (iv) require energy barriers of less than 2 eV to be surpassed and are expected to contribute more to the total electron transfer. DFT analysis reveals the interesting fact that the two frontier MOs (HOMO and LUMO) are not jointly involved in electron transfer. In the absence of primary orbital interactions, which usually dictate molecular reactivity, the imperative role of subjacent orbital effects[70–73] in the rate-determining step is established. The relative energies of the aforementioned sets

Table 4 Computationally derived d_{Re-O} (Å) and ρ_{BCP} (a.u.) values for all species appearing in Fig. 3 except **F** and **1**

Species	d_{Re-O} (Å)	ρ_{BCP} (a.u.)
A	1.695	0.2647
B	1.713	0.2516
C	1.722	0.2509
TS1	1.951	0.1446
D	2.176	0.0701
E	2.103	0.0786
TS2	2.209	0.0697
G	2.025	0.1187
TS3	2.264	0.0589
H	2.419	0.0367
I	2.139	0.0745

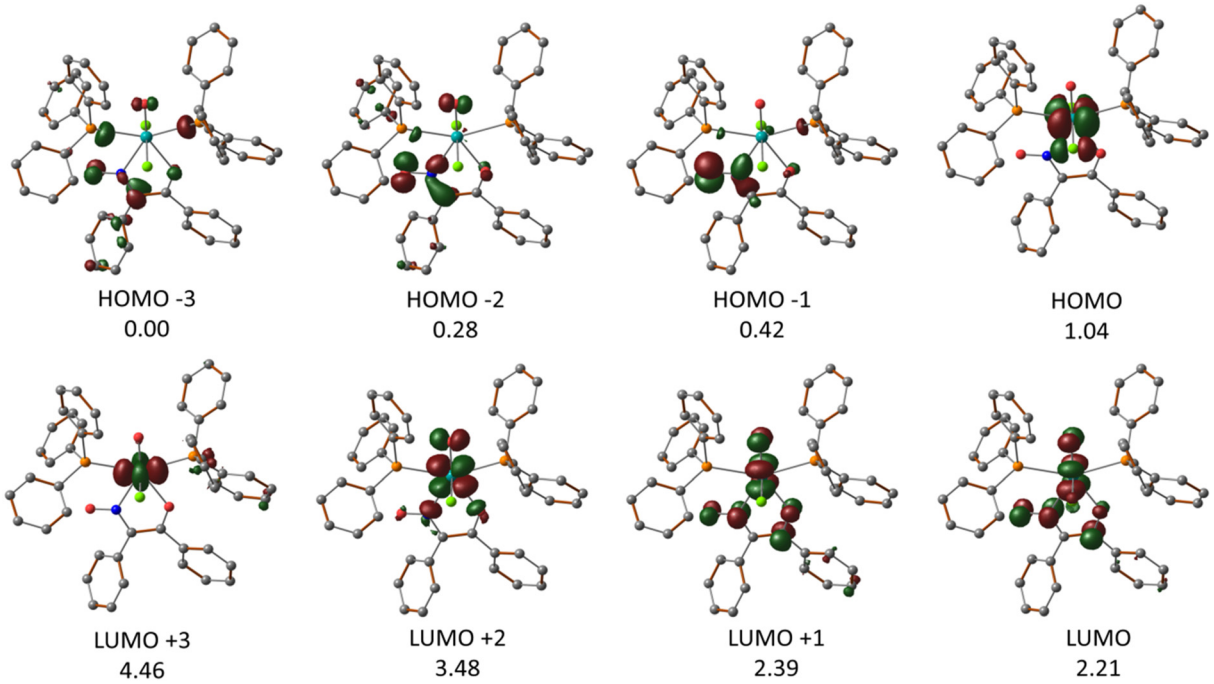

Fig. 5 Frontier and secondary molecular orbitals of **C** at an isosurface value of 0.06. The relative energies of the MOs are given in units of eV.

Table 5 Percentage contributions of some selected atomic orbitals to the MOs involved in the first OAT. The O, P1, and P2 atoms are bonded to rhenium in **C**, having bond lengths of 1.72, 2.60 and 2.65 Å, respectively

Energy feature		AO contribution (%)			
MO	ΔE (eV)	Re	O	P1	P2
LUMO+3	4.5	27.0	1.1	9.0	9.3
LUMO+2	3.5	50.7	18.2	0.9	2.2
LUMO+1	2.4	28.7	13.7	—	—
LUMO	2.2	27.0	13.8	—	—
HOMO	1.0	58.5	0.8	—	—
HOMO−1	0.4	3.4	0.8	6.1	4.0
HOMO−2	0.3	3.5	9.2	2.8	4.9
HOMO−3	0.0	1.4	4.0	8.0	9.4

of orbitals in **TS1** remain almost unaltered with respect to **C**, giving the impression that **TS1** and **C** are very much alike in their electronic aspects.

Metal-substrate selectivity of LNOH

Based on the mechanism elucidated by the intrinsic reaction coordinate study, $[Ph_3P–Re^{V}{\equiv}O]^{3+} \rightarrow [Re^{III}–OPPh_3]^{3+}$ two-electron intramolecular reduction seems to be a prerequisite for metal-promoted diaryl-α-ketooxime → diaryl-α-ketoimine functionalisation. Therefore, unraveling the fate of the dual deoxygenation reaction in response to inhibition of OAT-induced $Re^{V} \rightarrow Re^{III}$ reduction is indeed illuminating in the context of the experimental validation of the mechanism.

Aiming to verify our theory experimentally, we opted for an imidorhenium(v) precursor, $[Re^{V}(NC_6H_4Cl)Cl_3(PPh_3)_2]$, that incorporates a kinetically robust arylimido moiety in contrast to the labile oxo (O^{2-}) group present in the $[Re^{V}OCl_3(PPh_3)_2]$ substrate. If we rely on the proposed mechanistic pathway, it is clear that N–OH bond scission *via* oxidative addition will turn into an unlikely event without the initial OAT, and deoxygenation of LNOH straightway becomes infeasible. In fact, the deprotonation of LNOH is exclusively favoured with the imidorhenium(v) substrate, unlike the deoxygenation of LNOH observed in the case of the oxorhenium(v) substrate. The predominance of the C-nitroso form of LNO^{-} in **3** can impart substantial electronic inertness to the N–O bond in the Re^{V}–α-ketooximato complex, rendering the $O_{oximato}$ atom unresponsive to OAT.

Therefore, the coordination of diaryl-α-ketooxime to electron-rich Re^{III} at any intermediate stage is obligatory for the cleavage of the N–OH bond. Such experimental findings finally conclude that the N-functionalisation of LNOH into LNH is entirely oxorhenium(v)-substrate selective, while the O-functionalisation of LNOH into LNO^{-} is imidorhenium(v)-substrate selective.

Oxime-specific reaction course with $[Re^{V}OCl_3(PPh_3)_2]$

The striking difference between our report and Zubieta *et al.*'s report[8] is that the diaryl-α-ketooxime and salicylaldoxime (HONLOH, where OH is the phenolic group and NOH is the oxime group) ligands behave differently towards the $[Re^{V}OCl_3(PPh_3)_2]$ substrate, and the courses of the two reactions are entirely oxime specific (Scheme 2). In Zubieta *et al.*'s case, the structural integrity of the $[Re^{V}{\equiv}O]^{3+}$ moiety in the metal substrate is fully retained during the deoxygenation of

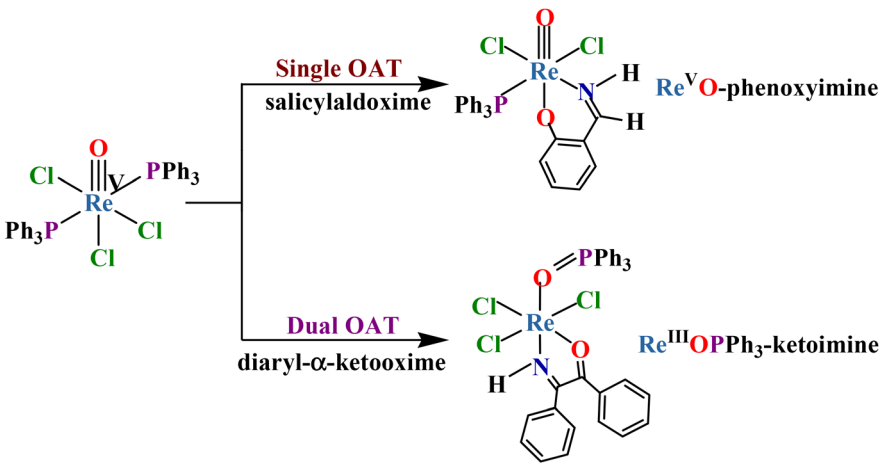

Scheme 2 A diagram of the contrasting reactions of salicylaldoxime and diaryl-α-ketooxime with the [Re^{V}OCl$_3$(PPh$_3$)$_2$] substrate.

HONLOH to afford the [O≡Re^{V}–phenoxyimine] product, whereas in our case, [Ph$_3$P–Re^{V}≡O]$^{3+}$ → [Re^{III}–OPPh$_3$]$^{3+}$ intramolecular reduction precedes the deoxygenation of LNOH to furnish the [Ph$_3$PO–Re^{III}–α-ketoimine] product. In an attempt to explain such fascinating reactivity contrast, a plausible mechanism for the Re^{V}-mediated deoxygenation of salicylaldoxime is developed based on necessary adjustments to the mechanism reported in our case, and this is portrayed in Scheme 3.

As the phenolic group of HONLOH is more acidic than the oxime group, the deprotonation of the former into an anionic phenolato form (HONLO^{-}) is preferred, and substitution of a chloride ion from [Re^{V}OCl$_3$(PPh$_3$)$_2$] by the nucleophilic phenolato–O atom should initiate the reaction. As a consequence, an η^1-O$_{phenolato}$-coordinated Re^{V} intermediate (**B′**) and HCl are yielded. Similar to **C** in Fig. 3, bidentate chelation of HONLO^{-} is subsequently completed in an η^2-N$_{oxime}$,O$_{phenolato}$ fashion to generate a heptacoordinated Re^{V}O species (**C′**). Geometry optimisation of **C′** at the M06-L/6-31G(d,p) level of theory, as implemented for **C**, reveals a distorted pentagonal bipyramidal structure, wherein two axial atoms are bent (∠Cl(axial)–Re–Cl (axial) = 165.1°) with respect to the skewed basal plane formed by the oxime, two PPh$_3$ groups and the oxo atom. The computed Re–O distance in the Re^{V}O motif in **C′** is 1.734 Å. The optimised N–OH length (1.397 Å) in **C′** is almost identical to the structurally characterised N–OH length (1.405 Å) of uncoordinated HONLOH.[74] The single-bond nature of the N–OH moiety implies that the lone pairs of the O$_{oxime}$ atom are localised. The two Re^{V}–PPh$_3$ bonds in **C′** are notably different: one is 2.570 Å long and the other has a length of 2.701 Å. Therefore, the longer Re^{V}–PPh$_3$ bond is susceptible to dissociation under appropriate activation.

A literature survey reveals that, apart from oxorhenium(v) complexes incorporating five/six-membered chelate rings[47–50,75–77] formed by neutral N-donors, other chelate rings featuring anionic O-donors cannot promote OAT from [Re^{V}≡O]$^{3+}$ to PPh$_3$ to form [Re^{III}–OPPh$_3$]$^{3+}$ derivatives. In the presence of an anionic O-donor in the primary coordination sphere, the effective positive charge on the metal is reduced, which thereby increases the energy of the π^{*}_{ReO} acceptor orbitals, hindering their access by PPh$_3$.[77] Therefore, monoanionic η^2-N$_{oxime}$,O$_{phenolato}$ coordination of HONLO^{-} to Re^{V} seems non-conducive to promote OAT. This impression is supported by the experimental observation that the allied phenolate and naphtholatepyrazole ligands react with [Re^{V}OCl$_3$(PPh$_3$)$_2$] to form only the Re^{V}O products[78,79] featuring η^2-N$_{pyrazole}$, O$_{phenolato}$ chelation, and no further OAT from the [Re^{V}≡O]$^{3+}$ core to PPh$_3$ is observed. Therefore, the formation of any Re^{III} derivative similar to that observed for diarl-α-ketooxime (**D** in Fig. 3) is a remote possibility in the case of HONLOH, and N–OH bond cleavage in **C′** *via* oxidative addition to the metal is unlikely.

Although PPh$_3$ does not lead to any oxygen atom abstraction from HONLOH under metal-free conditions, the modified electronic properties and spatial arrangements in a Re^{V}-bound state can trigger PPh$_3$-induced N–O bond cleavage. It is observed that the HO···PPh$_3$ nonbonded distance between the O$_{oxime}$ atom of the =N–OH motif and the P atom of the longer Re^{V}–PPh$_3$ bond is 2.851 Å in **C′**, which is nearly 0.5 Å less than the sum of the van der Waals radii of the O and P atoms.[67] Such proximity between the Re^{V}-bound =N–OH and PPh$_3$ groups in **C′** can therefore favour their mutual interaction. QTAIM analysis of **C′** reveals a bond critical point in between the two concerned O$_{oxime}$ and P atoms, and this is characterised by the quantum observables: ρ_{BCP} = 0.0181 a.u., $[V(r)|/G(r)]_{BCP}$ = 1.003 and $[H(r)/\rho(r)]_{BCP}$ = −0.002. The conditions, $[H(r)/\rho(r)]_{BCP} < 0$ and $[V(r)|/G(r)]_{BCP} > 1$, indicate that weak interaction[68,80] exists between the O$_{oxime}$ and P atoms in **C′**. Gradual strengthening of such an interaction along the O$_{oxime}$···P bond path eventually aids the formation of a *trans*-iminato species, [Re^{V}OCl$_2$(PPh$_3$)(η^2-OLN)]$^{-}$ (**H′**), which after isomerisation and proton transfer from [H–O=PPh$_3$]$^{+}$ forms the *cis*-imine species [Re^{V}OCl$_2$(PPh$_3$)(η^2-OLNH)], which remains hydrogen bonded with OPPh$_3$ (**I′**) in the gas phase.

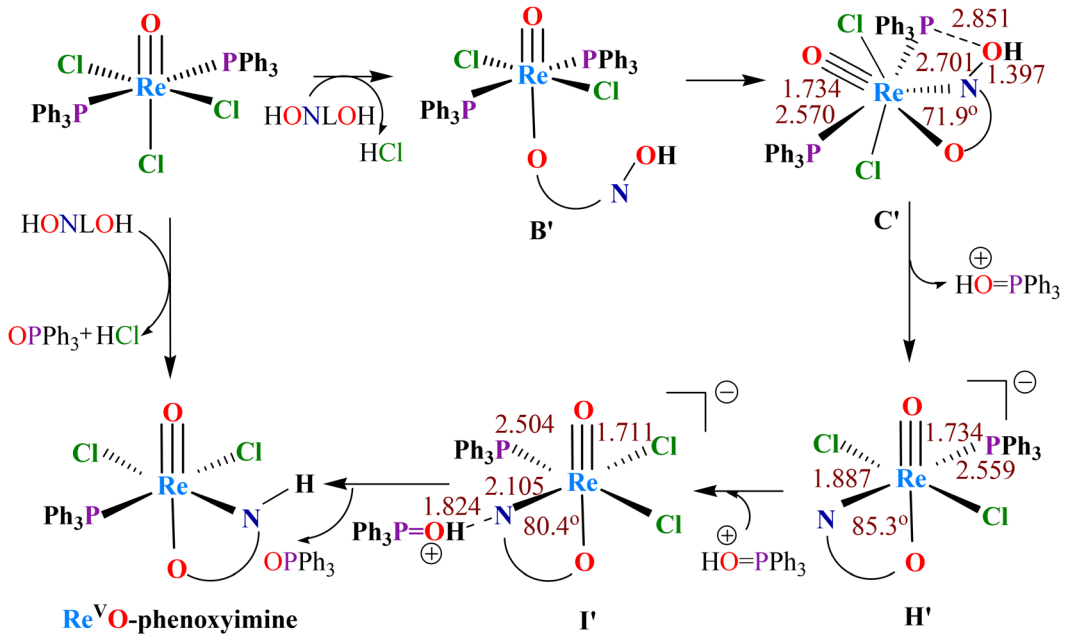

Scheme 3 A plausible pathway for the formation of [O≡Re^{V}–phenoxyimine] and $OPPh_3$ in the reaction between [Re$^{V}OCl_3(PPh_3)_2$] and salicylaldoxime.

During this iminato (**H′**) → imine (**I′**) functionalization, the Re≡O and Re–P bonds shrink by ~0.02 and ~0.06 Å, respectively, whereas the Re–N bond elongates by ~0.21 Å. A reduction in the bite angle of the oxime by ~5° also accompanies the changes in bond lengths. Finally, cleavage of the N–H···O hydrogen bond forms the [O≡Re^{V}–phenoxyimine] and $OPPh_3$ products.

Succinctly, the stronger Re–$O_{phenolato}$ bond in the case of salicylaldoxime pushes a higher electron density towards Re^{V} compared to the Re–O_{keto} bond in diaryl-α-ketooxime, which makes the $[Re^{V}{\equiv}O]^{3+}$ core less electrophilic toward PPh_3 in the former, inhibiting OAT. Thus, the non-accessibility of the Re^{III} state arrests subsequent oxidative addition for salicylaldoxime, unlike what is observed in this report. In the absence of any Re^{V}–OH intermediate for salicylaldoxime, N–OH bond cleavage instead involves an interaction between the Re^{V}-bound =N–OH and PPh_3 groups.

Conclusions

The reaction between [Re$^{V}OCl_3(PPh_3)_2$] and diaryl-α-ketooxime highlights the orchestrated interplay of intramolecular OAT, *trans* → *cis* isomerisation, *fac* → *mer* isomerisation, intramolecular oxidative addition, and proton transfer phenomena. The activation barriers for the two Re^{V}-centred OATs are profoundly different. The first OAT (**C** → **D**) involving intramolecular Ph_3P–Re$^{V}{\equiv}O$ → Re^{III}–$OPPh_3$ reduction is the slowest and is rate-determining in nature. PPh_3 manifests nucleophilic behaviour in the first OAT. Subjacent orbital effects in the rate-determining step help to accomplish the first oxygen atom transfer. The second intramolecular OAT (**G** → **H**) is kinetically facile due to an escalation in the nucleophilicity of the hydroxo group towards PPh_3 present in the Re^{V}–OH intermediate. PPh_3 behaves in an electrophilic manner in the second OAT. Interestingly, the roles of phosphine are reversed in the two intramolecular OAT events.

Preclusion of the first OAT in the imidorhenium(v) precursor inhibits the deoxygenation of diaryl-α-ketooxime. Instead, a Re^{V}–α-ketooximato complex is afforded *via* deprotonation. This implies that the N-functionalisation of diaryl-α-ketooxime is only possible at the Re^{III} centre as a result of the first OAT. The overwhelming contribution of the C-nitroso form of the oxime in the Re^{V}–α-ketooximato complex is asserted from structural analysis. The predominance of the C-nitroso form of any oxime, except diaryl-α-ketooxime, has not been reported earlier in rhenium chemistry.

As observed in the case of diaryl-α-ketooxime, metal-substrate selectivity towards deoxygenation and deprotonation is under scrutiny for dialkyl- and alkylaryl-substituted α-ketooximes. We hope that the expounded mechanism for double deoxygenation can effectively cast light on other examples of OAT-promoted functionalisation for different oximes.

Author contributions

A. S., S. B., A. D. and A. G. conducted the chemical experiments and data analysis. T. S. performed the DFT calculations related to the intrinsic reaction coordinate study and analysed the results with J. G. DFT calculations related to QTAIM, NBO and MBO studies were performed by S. S. and then analysed with J. G. T. N. performed the crystallographic studies. A. S.,

S. B., A. G., A. D., T. S. and J. G. contributed to writing, reviewing, and editing the manuscript. J. G. conceptualized the goals and aims of this work. All the authors gave approval to this version.

Conflicts of interest

There are no conflicts of interest to mention.

Data availability

Supplementary information: computational details and spectral observations. See DOI: https://doi.org/10.1039/d5dt01782c.

CCDC 2394051 (**1**) and 2394052 (**3**) contain the supplementary crystallographic data for this paper.[81a, b]

Acknowledgements

We wholeheartedly thank St. Paul's Cathedral Mission College, Kolkata, for providing the essential infrastructural facilities and other resources. We sincerely thank Dr. Soumya Ghosh, TIFR Hyderabad, India, for providing the computational resources to carry out this work. We thank the crystallographic reviewer of this paper for their generous help. T. S. gratefully acknowledges the Department of Atomic Energy, Government of India, and TIFR Hyderabad, India, for providing a postdoctoral fellowship. J. G. would like to express his deep sense of gratitude to Swami Divyananda Maharaj, Ex-Principal of Rahara Ramakrishna Mission Vivekananda Centenary College, Kolkata. J. G. wholeheartedly appreciates the constant motivation received from his daughter Adrija.

References

1 V. Y. Kukushkin, D. Tudela and A. J. L. Pombeiro, *Coord. Chem. Rev.*, 1996, **156**, 333–362.
2 V. Y. Kukushkin and A. J. L. Pombeiro, *Coord. Chem. Rev.*, 1999, **181**, 147–175.
3 C. J. Milios, T. C. Stamatatos and S. P. Perlepes, *Polyhedron*, 2006, **25**, 134–194.
4 D. S. Bolotin, N. A. Bokach, M. Ya. Demakova and V. Y. Kukushkin, *Chem. Rev.*, 2017, **117**, 13039–13122.
5 C. M. P. Cristina, M. F. C. Guedes da Silva, V. Y. Kukushkin, J. J. R. Frausto da Silva and A. J. L. Pombeiro, *J. Chem. Soc., Dalton Trans.*, 1998, 325–326.
6 G. Wagner, A. J. L. Pombeiro, A. N. A. Bokach and V. Y. Kukushkin, *J. Chem. Soc., Dalton Trans.*, 1999, 4083–4086.
7 L. Cuesta, M. A. Huertos, D. Morales, J. Perez, L. Riera, V. Riera, D. Miguel, A. M. Velazquez and S. Garcia-Granda, *Inorg. Chem.*, 2007, **46**, 2836–2845.
8 X. Chen, F. J. Femia, J. W. Babich and J. Zubieta, *Inorg. Chim. Acta*, 2000, **306**, 113–116.
9 I. Chakraborty, B. K. Panda, J. Gangopadhyay and A. Chakravorty, *Inorg. Chem.*, 2005, **44**, 1054–1060.
10 A. S. Belov, V. V. Novikov, G. E. Zelinskii, A. V. Vologzhanina, O. A. Varzatskii, B. F. Myasoedov and Y. Z. Voloshin, *Inorg. Chem. Commun.*, 2016, **72**, 23–29.
11 R. B. Singh, B. S. Garg and R. P. Singh, *Talanta*, 1979, **26**, 425–444.
12 J. C. Danilewicz, R. D. Guillard and R. Wootton, *Inorg. Chim. Acta*, 1975, **L5**, 15.
13 N. V. Thakkar and B. C. Haldar, *J. Inorg. Nucl. Chem.*, 1980, **42**, 843–849.
14 C. Natarajan and A. N. Hussain, *Transition Met. Chem.*, 1982, **7**, 252–257.
15 S. V. Salvi, P. H. Umadikar, M. R. Patil and P. M. Dhadke, *Spectrochim. Acta*, 1984, **39B**, 965–968.
16 H. Deligoz and M. Yilmaz, *Synth. React. Inorg. Met.-Org. Chem.*, 1996, **26**, 943–953.
17 P. S. Reddy and K. H. Reddy, *Polyhedron*, 2000, **19**, 1687–1692.
18 K. Ishihara, Y. Furuya and H. Yamamoto, *Angew. Chem., Int. Ed.*, 2002, **41**, 2983–2986.
19 K. Narasaka, H. Kusama, Y. Yamashita and H. Sato, *Chem. Lett.*, 1993, 489.
20 H. Kusama, Y. Yamashita and K. Narasaka, *Bull. Chem. Soc. Jpn.*, 1995, **68**, 373–377.
21 M. M. Abu-Omar and J. H. Espenson, *Inorg. Chem.*, 1995, **34**, 6239–6240.
22 M. M. Abu-Omar, E. H. Appelman and J. H. Espenson, *Inorg. Chem.*, 1996, **35**, 7751–7757.
23 M. M. Abu-Omar, L. D. McPherson, J. Arias and V. M. Béreau, *Angew. Chem., Int. Ed.*, 2000, **39**, 4310–4313.
24 Y. Zhang, K. D. Hurley and J. R. Shapley, *Inorg. Chem.*, 2011, **50**, 1534–1543.
25 J. A. Schachner, B. Terfassa, L. M. Peschel, N. Zwettler, F. Belaj, P. Cias, G. Gescheidt and N. C. Mösch-Zanetti, *Inorg. Chem.*, 2014, **53**, 12918–12928.
26 S. Raju, M. E. Moret and R. J. M. K. Gebbink, *ACS Catal.*, 2015, **5**, 281–300.
27 B. E. Scbultz, S. F. Gheller, M. C. Muetterties, M. J. Scott and R. H. Holm, *J. Am. Chem. Soc.*, 1993, **115**, 2714–2722.
28 R. Mayilmurugan, B. N. Harum, M. Volpe, A. F. Sax, M. Palaniandavar and N. C. Mosch-Zanetti, *Chem. – Eur. J.*, 2011, **17**, 704–713.
29 R. Hille, *Dalton Trans.*, 2013, **42**, 3029–3042.
30 G. W. Parshall, *Inorg. Synth.*, 1977, **17**, 110–111.
31 J. Chatt, J. D. Garforth, N. P. Jhonson and G. A. Rowe, *J. Chem. Soc.*, 1964, 1012–1020.
32 D. Michos, X. L. Luo, J. A. K. Howard and R. H. Crabtree, *Inorg. Chem.*, 1992, **31**, 3914–3916.
33 T. W. J. Taylor and M. S. Marks, *J. Chem. Soc.*, 1930, 2302–2307.
34 G. M. Sheldrick, *Acta Crystallogr., Sect. A:Found. Adv.*, 2015, **71**, 3–8.
35 G. M. Sheldrick, *Acta Crystallogr., Sect. A:Found. Crystallogr.*, 2008, **64**, 112–122.

36 G. M. Sheldrick, *SHELXL-2018*, Universität Göttingen, Göttingen, Germany, 2018.
37 O. V. Dolomanov, L. J. Bourhis, R. J. Gildea, J. A. K. Howard and H. Puschmann, *J. Appl. Crystallogr.*, 2009, **42**, 339–341.
38 M. J. Frisch, G. W. Trucks, H. B. Schlegel, G. E. Scuseria, M. A. Robb, J. R. Cheeseman, G. Scalmani, V. Barone, G. A. Petersson, H. Nakatsuji, X. Li, M. Caricato, A. V. Marenich, J. Bloino, B. G. Janesko, R. Gomperts, B. Mennucci, H. P. Hratchian, J. V. Ortiz, A. F. Izmaylov, J. L. Sonnenberg, D. Williams-Young, F. Ding, F. Lipparini, F. Egidi, J. Goings, B. Peng, A. Petrone, T. Henderson, D. Ranasinghe, V. G. Zakrzewski, J. Gao, N. Rega, G. Zheng, W. Liang, M. Hada, M. Ehara, K. Toyota, R. Fukuda, J. Hasegawa, M. Ishida, T. Nakajima, Y. Honda, O. Kitao, H. Nakai, T. Vreven, K. Throssell, J. A. Montgomery, J. E. Peralta, F. Ogliaro, M. J. Bearpark, J. J. Heyd, E. N. Brothers, K. N. Kudin, V. N. Staroverov, T. A. Keith, R. Kobayashi, J. Normand, K. Raghavachari, A. P. Rendell, J. C. Burant, S. S. Iyengar, J. Tomasi, M. Cossi, J. M. Millam, M. Klene, C. Adamo, R. Cammi, J. W. Ochterski, R. L. Martin, K. Morokuma, O. Farkas, J. B. Foresman and D. J. Fox, *Gaussian* 16, Revision C.01, Gaussian, Inc., Wallingford, CT, 2016.
39 Y. Zhao and D. G. Truhlar, *J. Chem. Phys.*, 2006, **125**, 194101.
40 W. J. Hehre, R. Ditchfield and J. A. Pople, *J. Chem. Phys.*, 1972, **56**, 2257–2261.
41 M. Dolg, U. Wedig, H. Stoll and H. Preuss, *J. Chem. Phys.*, 1987, **86**, 866–872.
42 Y. Zhao and D. G. Truhlar, *Theor. Chem. Acc.*, 2008, **120**, 215–241.
43 B. B. Averkiev and D. G. Truhlar, *Catal. Sci. Technol.*, 2011, **1**, 1526–1529.
44 D. G. Gusev, *Organometallics*, 2013, **32**, 4239–4243.
45 T. Lu and F. Chen, Multiwfn: A multifunctional wavefunction analyzer, *J. Comput. Chem.*, 2012, **33**, 580–592.
46 E. D. Glendening, J. K. Badenhoop, A. E. Reed, J. E. Carpenter, J. A. Bohmann, C. M. Morale, P. Karafiloglou, C. R. Landis and F. Weinhold, *NBO 7.0*, Theoretical Chemistry Institute, University of Wisconsin, Madison, 2018.
47 A. Sinha, J. Chakraborty, S. Banerjee and J. Gangopadhyay, *Polyhedron*, 2019, **171**, 112–119.
48 S. Sengupta, J. Gangopadhyay and A. Chakravorty, *Dalton Trans.*, 2003, 4635–4643.
49 S. Das, I. Chakraborty and A. Chakravorty, *Inorg. Chem.*, 2003, **42**, 6545–6555.
50 S. Das, I. Chakraborty and A. Chakravorty, *Polyhedron*, 2003, **22**, 901–907.
51 C. Klein, C. Fischer, W. Seichter, A. Schwarzer and E. Weber, *CrystEngComm*, 2011, **13**, 1931–1938.
52 G. V. Goeden and B. L. Haymore, *Inorg. Chem.*, 1983, **22**, 157–167.
53 W. A. Nugent and B. L. Haymore, *Coord. Chem. Rev.*, 1980, **31**, 123–175.
54 D. Beaudoin and J. D. Wuest, *Chem. Rev.*, 2016, **116**, 258–286.
55 D. Mansuy, P. Battioni, J. C. Chottard, C. Riche and A. Chiaroni, *J. Am. Chem. Soc.*, 1983, **105**, 455–463.
56 L. S. Wang, L. Chen, M. A. Khan and G. B. Richter-Addo, *Chem. Commun.*, 1996, 323–324.
57 L. Chen, M. A. Khan, G. B. Richter-Addo, V. G. Young Jr. and D. R. Powell, *Inorg. Chem.*, 1998, **37**, 4689–4696.
58 S. C. Chan, H. Y. Cheung and C. Y. Wong, *Inorg. Chem.*, 2011, **50**, 11636–11643.
59 A. I. Mikhaleva, A. B. Zaitsev and B. A. Trofimov, *Russ. Chem. Rev.*, 2006, **75**, 797–823.
60 H. Y. Jin, S. Ikari, K. Kobayashi, K. Umakoshi, H. Sugimoto, A. Mitani, M. Abe, Y. Sasaki and T. Ito, *Bull. Chem. Soc. Jpn.*, 2004, **77**, 1139–1146.
61 C. M. Che, Y. P. Wang, K. S. Yeung, K. Y. Wonga and S. M. Peng, *J. Chem. Soc., Dalton Trans.*, 1992, 2675–2677.
62 L. Xu, I. A. Setyawati, J. Pierreroy, M. Pink, V. G. Young Jr., B. O. Patrick, S. J. Rettig and C. Orvig, *Inorg. Chem.*, 2000, **39**, 5958–5963.
63 N. D. McMillion, Q. J. Bruch, C. H. Chen, F. Hasanayn and A. J. M. Miller, *Dalton Trans.*, 2023, **52**, 15115–15123.
64 W. A. Nugent and J. A. Mayer, *Metal-Ligand Multiple Bonds*, Wiley, New York, 1988, ch. 5.
65 R. Reed, L. A. Curtiss and F. Weinhold, *Chem. Rev.*, 1988, **88**, 899–926.
66 R. F. W. Bader, *Atoms in Molecules, a Quantum Theory*, Oxford University Press, Oxford, UK, 1990.
67 M. Mantina, A. C. Chamberlin, R. Valero, C. J. Cramer and D. G. Truhlar, *J. Phys. Chem. A*, 2009, **113**, 5806–5812.
68 S. Sen, A. Sinha, S. Banerjee, S. Debnath, A. Ghosh, J. Chakraborty and J. Gangopadhyay, *ACS Omega*, 2024, **9**, 22476–22487.
69 P. Muller, *Subjacent orbital in IUPAC Compendium of Chemical Terminology, International Union of Pure and Applied Chemistry*, 5th edn, 2025. Online version 5.0.0. 2025. DOI: 10.1351/goldbook.S06067.
70 J. Cipressi and S. N. Brown, *Chem. Commun.*, 2014, **50**, 7956–7959.
71 J. A. Berson and L. Salem, *J. Am. Chem. Soc.*, 1972, **94**, 8917–8918.
72 N. D. Epiotis, R. L. Yates and F. Bernardi, *J. Am. Chem. Soc.*, 1975, **97**, 4198–4202.
73 B. J. Levandowski, D. Svatunek, B. Sohr, H. Mikula and K. N. Houk, *J. Am. Chem. Soc.*, 2019, **141**, 2224–2227.
74 C. E. Pfluger and R. L. Harlow, *Acta Crystallogr., Sect. B*, 1973, **29**, 2608–2609.
75 S. Banerjee, S. Bhattacharyya, B. K. Dirghangi, M. Menon and A. Chakravorty, *Inorg. Chem.*, 2000, **39**, 6–13.
76 S. Bhattacharyya, I. Chakraborty, B. K. Dirghangi and A. Chakravorty, *Inorg. Chem.*, 2001, **40**, 286–293.
77 S. B. Seymore and S. N. Brown, *Inorg. Chem.*, 2000, **39**, 325–332.
78 P. Traar, J. A. Schachner, L. Steiner, A. Sachse, M. Volpe and N. C. Mösch-Zanetti, *Inorg. Chem.*, 2011, **50**, 1983–1990.

79 N. Zwettler, J. A. Schachner, F. Belaj and N. C. Mösch-Zanetti, *Inorg. Chem.*, 2014, **53**, 12832–12840.
80 E. Espinosa, I. Alkorta, J. Elguero and E. Molins, *J. Chem. Phys.*, 2002, **117**, 5529–5542.
81 (*a*) CCDC 2394051: Experimental Crystal Structure Determination, 2025, DOI: 10.5517/ccdc.csd.cc2lc6gn; (*b*) CCDC 2394052: Experimental Crystal Structure Determination, 2025, DOI: 10.5517/ccdc.csd.cc2lc6hp.